WARM PRESTRESSING OF BLUNT NOTCHES

C.P. Harris*, P. Bowen* and J.F. Knott*

The phenomenon of warm prestressing (WPS) has been studied using blunt-notched testpieces. It is shown that WPS operates for both load-cool-fracture (LCF) and load-unload-cool-fracture (LUCF) sequences. For the LUCF sequence it is possible to demonstrate the role of residual stress by prestressing with the notch either in tension or in compression. For both LCF and LUCF sequences, it is necessary to produce new plasticity on reloading, at a temperature lower than the WPS temperature.

INTRODUCTION

The plane-strain fracture toughness (K_{IC}) of a ferritic steel generally exhibits a strong temperature dependence: increased values of K_{IC} are measured as the test temperature is increased. This temperature dependence of K_{IC} allows the important phenomenon known as "warm prestressing" (WPS) to occur. Here, the fracture toughness of a material at low temperature can be increased if it is first subjected to stress at a higher temperature. This is illustrated schematically in figure 1. Two kinds of WPS cycle are considered. The load-cool-fracture (LCF) cycle loads a pre-cracked piece to a load at high temperature, greater than the fracture load at low temperature. If the temperature is then decreased to the lower value (sufficiently carefully to prevent the introduction of thermal stresses) it is found that the load must be increased to a value greater than the prestress load before fracture occurs. In the load-unload-cool fracture (LUCF) cycles, the prestress load is removed at the higher temperature and the testpiece is cooled to the lower temperature before reloading. The fracture load at low temperature is now found to be greater than that for a testpiece

*Department of Metallurgy and Materials Science,
University of Cambridge.

not subjected to any WPS cycle but, in general, not as high as the prestress load.

The aims of theories of WPS should be to predict the increase in fracture load above the prestress load for an LCF cycle and to predict the fracture load for an LUCF cycle. Factors which must be incorporated are the effects of macroscopic, pre-crack blunting during the prestressing; the generation of residual stress on unloading; and the blunting-out of microcrack nuclei, formed in microstructural features, such as carbides or inclusions. In this last case, it would be necessary to generate new plasticity at the low temperature to nucleate fresh microcracks. Models for WPS, based on superposition of stress fields, have been developed and used by Chell (1) and Curry (2).

It appeared that several of the factors affecting the WPS phenomenon could be addressed through a study of behaviour in blunt-notched testpieces. First, the change in notch profile during prestressing should have minimal effect on subsequent low-temperature fracture, which initiates below the notch. Secondly, it is possible to prestress with the notch either in tension or in compression, so that the sign of the residual stress in an LUCF cycle can be changed (see fig.2). Thirdly, no ambiguities arise, concerning the effect of a room-temperature fatigue precracking procedure on subsequent low-temperature fracture. The notch geometry chosen was one for which elastic-plastic stress analyses were available (Griffiths and Owen (3), Wall and Foreman (4)). These analyses give details of the stress and strain distributions ahead of the notch root, and have greatly facilitated recent investigations into the micro-mechanisms of cleavage fracture (Bowen, Druce and Knott (5), Bowen and Knott (6)). For cleavage fracture the critical event can be observed (McRobie (7), Bowen et al (8)) or deduced (5) to occur at positions of peak tensile stress. This value of peak tensile stress is conventionally known as the microscopic (local) cleavage fracture stress, σ_F^*. The positions of peak tensile stress below the notch root are shown in fig.3, after (3).

This paper reports on some detailed observations of warm prestressing in blunt notches.

EXPERIMENTAL METHODS

Tests were performed on three varieties of pressure-vessel steel:
(a) commercial A508 Class 3 ring forging, supplied in a fully-tempered condition;
(b) A533B plate, (grade 1), heat-treated to give a coarse-grained, lightly-tempered, martensitic microstructure (austenitised at 1250°C for 1h, oil-quenched, tempered at 290°C for 1h, air-cooled);
(c) A533B plate, (grade 2), as-received in a non-fully tempered condition.

The chemical compositions of these steels are given in Table 1.

TABLE 1 - Chemical compositions, wt%

	C	Mn	Ni	Mo	Si	Cr	Cn	P	S
A508 class 3	0.17	1.50	0.78	0.53	0.28	0.28	0.06	0.006	0.011
A533B(grade 1)	0.25	1.51	0.63	0.53	0.22	0.06	0.04	0.005	0.005
A533B(grade 2)	0.19	1.55	0.62	0.51	N.A	N.A	N.A	N.A	N.A

N.A. = not analysed

The notched-bar geometry shown in fig.2, conforms to that used by Griffiths and Owen (3) for their finite-element stress analysis. The A508 specimens were machined in the LS (longitudinal-short-transverse) orientation and the A533B specimens were machined in the TL (transverse-longitudinal) orientation. Fracture tests were carried out in four-point bending over the temperature range -196 to -100°C, using a 100kN Mand servohydraulic testing machine. Temperature control to ± 5 °C was maintained in all tests. The measured fracture loads for the three steels investigated are shown in figs.4,5 and 6. It is observed that they increase with increasing test temperature. Tensile properties were evaluated over the temperature range -196 to +20°C. Values of the 0.2% proof stresses for the three steels are shown in fig.7. Large variations in 0.2% proof stress are observed, and these variations reflect the different microstructural conditions produced by the prior heat-treatments.

From the measured fracture load, P_F, and the 0.2% proof stress it is possible to determine the value of σ_F* in the following way. The value of P_F defines the nominal bending stress, σ_{nom}, at failure through:

$$\sigma_{nom} = M/B(W-a)^2 \quad \text{.....................................(1)}$$

where M is the applied bending moment, W is the testpiece width and a is the notch depth. Using the Griffiths-Owen stress intensification analysis, fig.8, it is then possible to determine values of σ_F* (see Table 2). For the three conditions these values are shown as a function of temperature in fig.9. A number of points may be noted from this figure.

Firstly, consider the temperature dependence of σ_F* observed in the three different conditions. In the high-strength martensitic condition, the value of σ_F* is observed to be relatively constant

at 3400 ±200MPa over the temperature range -160 to -100°C, and to fall to a value of 2800 MPa at -196°C. This trend is similar to that observed previously in martensitic microstructures (6). In the non fully tempered A533B (grade 2), σ_F^* is observed to be temperature independent at 2250 ±100 MPa, over the temperature range -196 to -150°C. In the fully-tempered A508 steel, the mean value of σ_F^* obtained at -140°C is 1560 MPa, and at-196°C the mean value of σ_F^* obtained is 1900 MPa. These values tend to suggest an increase in σ_F^* at -196°C, but it should be noted that for three of the six testpieces fractured at -140°C only lower bound values to σ_F^* of 1600 MPa can be quoted. For these testpieces, at fracture the value of $\sigma_{nom}/\sigma_{0.2}$ exceeded 2.31, which is the limit to the finite element analysis - fig.8. [It is of interest to note that an upper limit to the value of σ_F^* at -140°C can be estimated as 1810 MPa]. It can be seen that the temperature dependence of σ_F^* over the range -196 to -160°C (in particular) is different for different microstructures.

TABLE 2 - Summary of cleavage fracture behaviour in blunt notch tests performed at -196°C

Specimen	Failure load (kN)	σ_{nom} (MPa)	$\sigma_{0.2}$ (MPa)	$\sigma_{nom}/\sigma_{0.2}$	R	σ_F^* (MPa)
A3	27.4	1240	900	1.38	2.16	1940
B3	23.9	1090	900	1.21	2.04	1840
C3	24.8	1130	900	1.26	2.08	1870
A4	27.5	1250	900	1.38	2.16	1940
B4	29.3	1330	900	1.48	2.20	1980
C4	27.0	1230	900	1.36	2.13	1920

Secondly, consider the mean values of σ_F^* obtained for the martensitic A533B and fully tempered A508 conditions. These are approximately 3400 and approximately 1800 MPa respectively. The 0.2% proof stresses measured for the martensitic condition are, of course, substantially higher than those measured for the fully-tempered condition - fig.7. Since the value of σ_F^* characterises the local "toughness", this observed trend in σ_F^* values is at first sight unusual, because fracture toughness is generally observed to decrease with increasing yield stress. The important point, however, is that both σ_F^* and K_{IC} (and $\sigma_{0.2}$) are all controlled by the same microstructural feature, previously established as carbide size (5). The martensitic condition which

exhibits the highest σ_F* values has a coarsest carbide width of 100nm (5) and the fully tempered (A508) condition which exhibits the lowest σ_F* values has a coarsest carbide width of $\gtrsim 1\mu$m. This is consistent with the previously proposed critical influence of carbide size on cleavage fracture (5).

Having considered the cleavage fracture behaviour without WPS it is now necessary to consider the effects of WPS. Both LCF and LUCF cycles have been examined. It is appropriate first to treat the LCF cycle.

The LCF Cycle in A508

Warm prestressing was carried out at temperatures of either 20°C or -140°C, with final fracture at -196°C. The prestress load at both 20°C and -140°C was calculated to give the same ratio of nominal bending stress to yield stress, ie $\sigma_{nom}/\sigma_{0.2} = 2.23$.

The fracture load at -196°C for a testpiece not subjected to WPS is 26.7kN with a scatter-band of ±2.6kN (see Table 2). This is increased to a mean load of 32kN with a scatter-band of ±1.5kN if a WPS load of 23kN (ie $\sigma_{nom}/\sigma_{0.2} = 2.23$) is applied at 20°C (see Table 3).

TABLE 3 - LCF sequences for A508 testpieces prestressed to general yield and cooled under load to -196°C

Specimen	Prestressing operations (All loads in kN)	Prestress-temperature °C	Subsequent fracture load (kN) at -196°C
C10	Load to +23.0	+20	31.3
B8	Load to +23.0	+20	32.9
C6	Load to +30.6	-140	33.3
C7	Load to +30.2	-140	32.2
C11	Load to +29.9	-140	30.2

An increase to a similar fracture load is obtained from a WPS load of 30kN (ie $\sigma_{nom}/\sigma_{0.2} = 2.23$) applied at -140°C (see Table 3). Therefore it is apparent that a WPS effect can be obtained in blunt notched testpieces and, moreover, that it is the fraction of general yield, rather than the absolute value of load, achieved during WPS, that is important. [Note that the size of the plastic zone ahead of a blunt notch is constant for a given fraction of general yield (3)]. It is intriguing that the WPS load applied at 20°C (23kN) is

less than the lowest value of fracture load at -196°C observed for a testpiece not subjected to the WPS treatment (see Table 2). The conventional schematic diagram shown in fig.1, is therefore not completely satisfactory for describing the WPS effects in blunt notches. A more complete illustration of the LCF results in blunt notches is shown in fig.10.

These results are in broad agreement with Chell's theory of WPS for pre-cracked testpieces (1), which emphasises the need to produce new plasticity at the lower temperature. There are, however, differences in detail between the blunt-notch and sharp-crack situation. One conclusion is that the need to incorporate macroscopic crack-tip blunting in a general theory of WPS is seen to be unnecessary because WPS has been observed here for notches, where the changes in notch-root radius are minimal. In addition, a sharply pre-cracked specimen has a very high elastic stress-concentration at the crack-tip, so that, for a LCF cycle, the enhancement of fracture load above the WPS load is predicted to be small because (a) only a small increase in load is required to produce new plastic flow and (b) the stress peak ahead of the pre-crack immediately attains its full value (typically of the order of five times the appropriate proof stress (9)) and will be sufficient to cause failure at the lower temperature, (where $\sigma_{0.2}$ has increased). For a notch of the root radius used in the present work, the maximum elastic stress concentration is $4.15\sigma_{nom}$ (after Kfouri(10)) - see fig.11. Therefore, if new plasticity is required to promote failure at the lower temperature, the applied load has to be increased above the WPS load by a discrete amount, conventionally, until the 0.2% proof stress at -196°C is attained at the notch surface. Moreover, the region in which new plasticity is first generated will be at the notch root, which is not the position of peak tensile stress present ahead of the notch root (from fig.3, for $\sigma_{nom}/\sigma_{0.2} = 2.23$, this position occurs at a distance of approximately 2.5ρ). It is not self evident for the blunt-notch situation, therefore, that increasing the applied load to a level such that the notch-root stress is equal to the 0.2% proof-stress at -196°C will be sufficient to promote failure. Indeed, still further increases may be necessary either to generate sufficiently high stresses within this reyielded active plastic zone close to the notch root to meet the local value of σ_F^*, or to spread yielding into regions where peak tensile stresses (at approximately 2.5ρ) already exist and the fracture is mechanism-controlled (Cottrell (11)). [This situation is fundamentally different to that existing for the sharp-crack, because the peak tensile stress occurs very close to the sharp-crack tip, where yielding is also favoured (by the high elastic stress concentration). Therefore, on application of a small fractional load, in a sharp-crack testpiece, local yielding can promote failure].

The observations of the present study allow the following distinctions to be drawn.

Consider first the testpieces prestressed to 30kN at -140°C. Note, that for some testpieces, this prestress load is sufficient to cause catastrophic cleavage fracture - see fig.4. After cooling to -196°C, the minimum extra applied load required to promote failure is 0.3kN - see Table 3. Even allowing for a stress concentration of $4.15\sigma_{nom}$ (fig.11), this extra applied load gives a local stress of only 60 MPa. This local stress is insufficient to promote "local" macro yielding, i.e. the total stress is still less than the 0.2% proof-stress at -196°C. (The same trend is observed in general for the martensitic condition - see Table 4). It would appear, therefore, that for testpieces in which the prestressing load (at the higher temperature) is greater than the fracture load of a testpiece not subjected to WPS (at the lower temperature), it is possible that, as a lower bound, only local micro-plasticity is required to promote failure. Failure is then under mechanism control and must occur close to the root of the notch. More typically in a LCF cycle the extra applied load required to promote failure at -196°C is between 2-3kN (see Table 3). Using fig.11, it is now evident that new plasticity occurs to a distance of $0.3\text{-}0.5\rho$ ahead of the notch prior to failure. From fig.12, this increased plasticity will "unlock" higher tensile stresses present ahead of the notch root, and the results are consistent with a mechanism-controlled fracture criterion modified to take account of local regions of increased tensile stress.

TABLE 4 - LCF sequences for high strength martensitic A533B testpieces. Prestressing was performed at 20°C to varying fractions of general yield. Subsequent fracture was at -196°C.

Specimen	Prestressing operations (All loads in kN)	Prestress-temperature °C	Subsequent fracture load (kN) at -196°C
M1	Load to +39.6	+20	40.1
M2	Load to +49.0	+20	49.1
M3	Load to +56.7	+20	66.9
M4	Load to +63.4	+20	64.0

Consider second the testpieces prestressed to 23.0kN at 20°C. The peak tensile stresses "locked" in during cooling to -196°C are shown in fig.12. Note that this peak value of tensile stress locked in at 20°C is lower than that locked in at -140°C. The subsequent failure at -196°C, required an increased load of approximately 8kN - Table 3. Using fig.11, the reyielded zone extends to a distance of 1.5ρ ahead of the notch root. It is of

interest to observe from fig.12 that the tensile stress "locked" in at a distance of 0.3-0.4ρ by prestressing at -140°C, is closely similar to that locked in at a distance of 1.5ρ by prestressing at 20°C. Therefore, although the results are consistent with a mechanism-controlled fracture criterion, the importance of the spatial distribution of tensile stress below the notch root must be emphasised.

The LUCF Cycle

Two types of experiment have been performed. Both involve LUCF sequences in tension and compression as follows: in A508 testpieces WPS to the same fraction of general yield at -140 and 20°C; in A533B testpieces different levels of WPS at a single test temperature, 20°C.

LUCF Cycles in A508

These involve prestressing to a single value of $\sigma_{nom}/\sigma_{0.2}$ = 2.23 as described for the LCF cycle, either in tension or in compression(fig.2). It is important to note that previous research has shown that the general yield load is closely similar in both tension and compression (12). Compressive prestress was performed at the temperatures of -140 and 20°C, but tensile prestress only at -140°C. The results are given in Table 5. For the tensile LUCF sequence a small improvement from a fracture load of 26.7 ±2.6kN for testpieces not subjected to WPS, to a fracture load of 27.6 ±0.6kN is observed. This failure load is less than the prestress load.

For the compressive LUCF, dramatic decreases in subsequent failure load from a value of 26.7 ±2.6kN for testpieces not subjected to WPS, to a value of 11.1 ±1.3kN is observed. Similar decreases of subsequent fracture load are observed when compressive WPS is performed at -140 and 20°C. This indicates (a) the importance of the fraction of general yield to which testpieces are prestressed rather than the absolute level of prestressing load (as for the LCF cycles), (b) the importance of the residual stress distribution.

From these results, it is clear that the residual tension (from compressive WPS) is much more effective in decreasing the subsequent fracture load at -196°C, than is the residual compression (from tensile WPS) in increasing the subsequent fracture load at -196°C - Table 5. This intriguing observation can be explained by the fact that the position of peak tensile stress moves progressively further away from the notch root as the fracture load, P_F (and hence σ_{nom}) increases - see fig.3. By analogy with the sharp crack situation (and supported experimentally by multiple load-unload cycles at -140°C (13)) it may be deduced that the highest residual stresses will be generated close to the notch root.

TABLE 5 - LUCF sequences for A508 testpieces prestressed to general yield, unloaded at the prestress temperature, and tested to failure at -196°C. Note testpieces have been loaded to general yield either in tension, or in compression. Compressive prestressing dramatically reduces the subsequent fracture load at -196°C.

Specimen	Prestressing operations (All loads in kN)	Prestress-temperature °C	Subsequent fracture load (kN) at -196°C
C8	Load to +30.5, unload	-140	28.2
B13	Load to +29.4, unload	-140	27.0
C10	Load to -30.6, unload	-140	11.8
B10	Load to -29.8, unload	-140	9.7
A7	Load to -22.8, unload	+20	11.1
A10	Load to -23.1, unload	+20	11.8

The local tensile residual stresses (from compressive WPS) will then superimpose on the load (stress) applied at -196°C and promote failure close to the notch root at a low applied load (11kN). The compressive residual stresses (from tensile WPS) will certainly prevent failure close to the notch root, but as the peak applied tensile stress moves progressively away from the notch root (and increases in value - fig.3) the compressive residual stresses will begin to decrease in magnitude. A quantitative assessment of this effect requires the residual stress distributions to be evaluated using elastic-plastic analysis, but the schematic distribution of residual stresses shown in fig.13, is consistent with the experimental results on A508.

LUCF Cycles in A533B

(A) Non fully tempered A533B. From Fig.14, the trend of subsequent failure load is observed to be similar to that observed in fully tempered A508. If tensile WPS is performed to general yield at 20°C, then the subsequent fracture load at -196°C increases from a load of 33 ±3kN (unprestressed testpiece) to 39kN. Compare this increase in fracture load with the decrease observed after compressive WPS from 33 ±3kN to 8kN (fig.14). A small reduction in fracture load from 33 ±3kN to 26kN is measured if a warm pre-stressing compressive load of 16kN is applied. No beneficial effects are observed if a warm prestressing tensile load of up to

33kN is applied. Again, little of a quantitative nature may be deduced in the absence of elastic/plastic analysis for the unloading cycle, but it is inferred that the important factor which controls the subsequent fracture load is the distance over which the residual stress distribution is maintained relative to the position and magnitude of the peak of the applied tensile stress.

(B) Martensitic A533B. It is observed that the trend in subsequent fracture load is observed to be similar after both tensile WPS or compressive WPS, i.e. the reduction in failure load observed after compressive WPS, 30 to 15kN, is closely similar to the increase in failure load observed after tensile WPS, 30 to 45kN - fig.15. This result is surprising in view of the earlier observations on the lower strength conditions. It must be emphasised, however, that for this high strength condition, in testpieces not subjected to WPS, at -196°C the value of $\sigma_{nom}/\sigma_{0.2} \simeq 0.80$ at failure. For the fully-tempered, A508, low strength condition, in testpieces not subjected to WPS, at -196°C the value of $\sigma_{nom}/\sigma_{0.2}$ at failure is in the range 1.21-1.48 (Table 2). From fig.3, it is therefore apparent that the peak of tensile stress occurs closer to the notch root in the high strength condition than in the low strength condition. It is plausible that the compressive residual stresses are now likely to be relatively more effective in delaying the onset of catastrophic failure (and indeed yielding), and larger increases in fracture load would then be expected and are observed experimentally. This emphasises, once again, the importance of the position of the peak of applied tensile stress relative to the position of high residual stresses in determining the final fracture load after WPS.

In summary, for LUCF sequences, the residual stress distribution is deduced to be of crucial importance in determining the subsequent fracture load (at -196°C). It appears that the value of σ_F^* is then achieved by the superposition of the residual and applied tensile stresses.

It should be instructive to examine such WPS effects in weld-metals, because actual cleavage initiation sites can often be observed ahead of blunt-notches (7,8).

CONCLUSIONS

The research has investigated some effects of warm prestressing (WPS) in blunt-notched testpieces, which were chosen to assess critical factors in the mechanisms of WPS.

(1) It has been established that WPS occurs in blunt-notched test-pieces for both load-cool-fracture (LCF) and load-unload-cool-fracture (LUCF) sequences.
(2) The LCF sequence demonstrates the need to produce new plasticity prior to fracture at the lower temperature.

(3) By applying WPS in either tension or compression, it has been shown that the sign of the residual stress on unloading has a strong effect on the subsequent fracture load at low temperature: pre-stressing in tension increases the fracture load; prestressing in compression reduces the fracture load. This effect has been analysed in terms of a superposition of residual and applied stress fields.
(4) It is observed that an increase in subsequent fracture load can be obtained, even when the WPS load at high temperature is less than the low temperature fracture load of a testpiece not subjected to any WPS sequence. The most important factor appears to be the amount of strain injected during warm prestressing.

ACKNOWLEDGEMENTS

Support for one of the authors (CPH) by a grant from CERL is gratefully acknowledged. During the course of the work one of the authors (PB) was supported by a Goldsmiths' Junior Research Fellowship at Churchill College, Cambridge. Additional support from AERE, Harwell is also gratefully acknowledged. Thanks are due to Professor D. Hull for provision of laboratory facilities.

REFERENCES

(1) Chell, G.G., Proc. 4th Internat. Conf. Pressure Vessel Technology, Vol.1, pp 117, Inst. Mech. Eng., London, 1980.

(2) Curry, D.A., CERL Report No.RD/L/N 103/79, CERL, Leatherhead, U.K., 1979.

(3) Griffiths, J.R. and Owen, D.R.J., J. Mech. Phys. Sol., Vol.19, 1971, pp 419-431.

(4) Wall, M. and Foreman, A.J., Harwell Report, R11618, UKAEA, 1985.

(5) Bowen, P., Druce, S.G., and Knott, J.F., in press Acta. metall., 1986.

(6) Bowen, P. and Knott, J.F., Met. Sci., Vol.18, 1984, pp 225-235.

(7) McRobie, D.E., Ph.D. Thesis, "Cleavage Fracture in C-Mn Weld Metals", University of Cambridge, 1985.

(8) Bowen, P., Ellis, M.B.D., Strangwood, M., and Knott, J.F., ECF6 (this conference), 1986.

(9) Rice, J.R. and Johnson, M.A., "Inelastic behaviour of solids", pp 541, 1970 (ed. M.F. Kanninen et al) McGraw Hill, New York.

(10) Kfouri, A.P., Ph.D. Thesis, "The elasto-plastic analysis of continua by Finite Element Methods", University of Cambridge 1970.

(11) Cottrell, A.H., Trans. Am. Inst. Min. Metall. Petrol. Engrs, Vol.212, pp 192-203, 1958.

(12) Knott, J.F. and Cottrell, A.H., J.I.S.I., Vol.201, pp 249-260, 1963.

(13) Bowen, P. and Knott, J.F., submitted to Int. Journ. Fracture 1986.

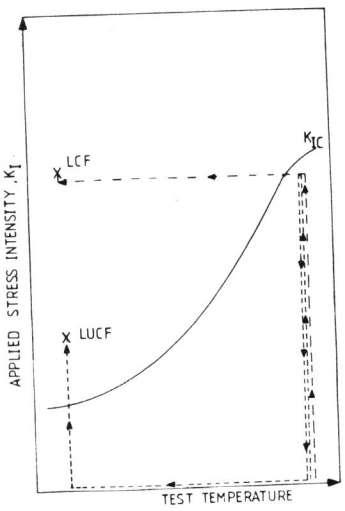

Fig. 1 Conventional schematic diagram illustrating WPS.

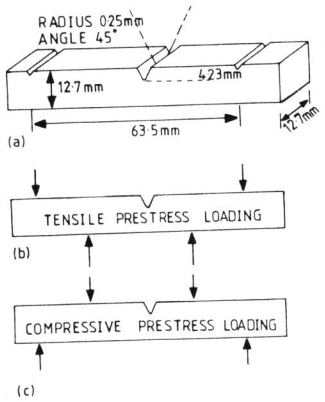

Fig. 2(a) Testpiece geometry; (b), (c) loading configurations.

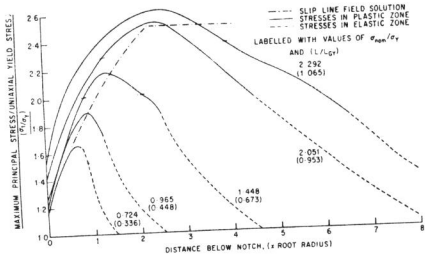

Fig. 3 Variation of maximum principal tensile stress below notch root, with applied load (after 3).

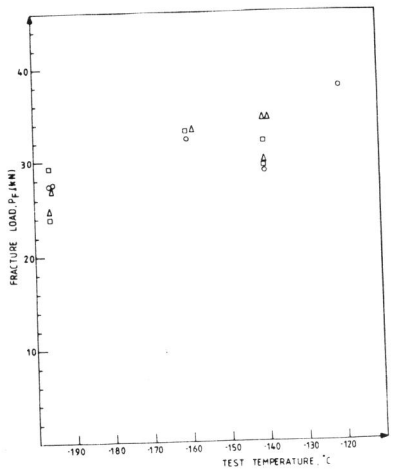

Fig. 4 Variation of fracture load with test temperature (A508).

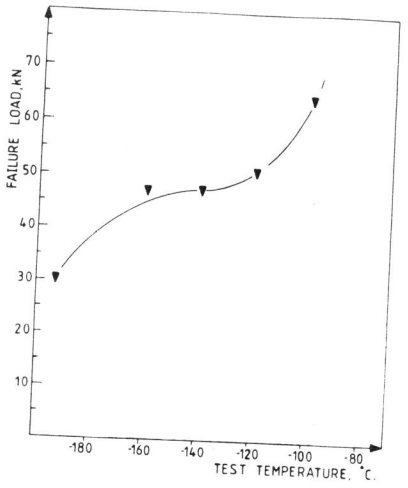

Fig. 5 Variation of fracture load with test temperature (martensitic A533B).

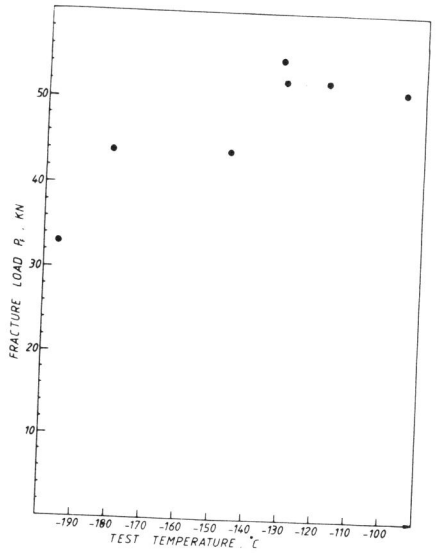

Fig. 6 Variation of fracture load with test temperature (A533B-non-fully tempered condition).

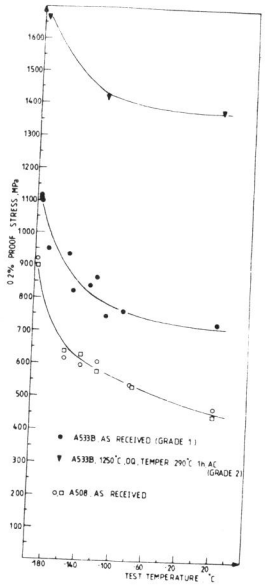

Fig. 7 Variation of 0.2% proof stress with temperature.

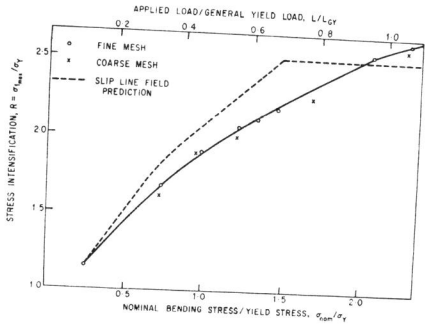

Fig. 8 Variation of maximum tensile stress intensification with applied load (after 3).

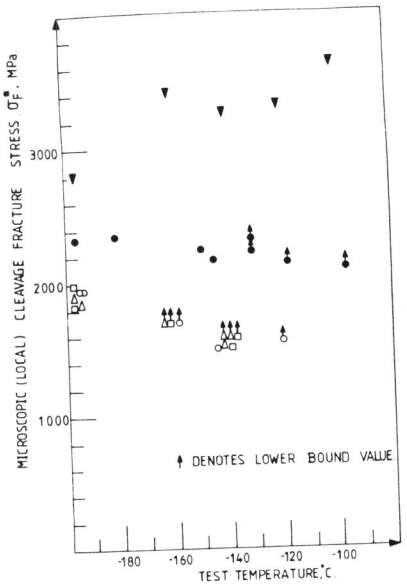

Fig. 9 Variation of σ_F^* with test temperature.

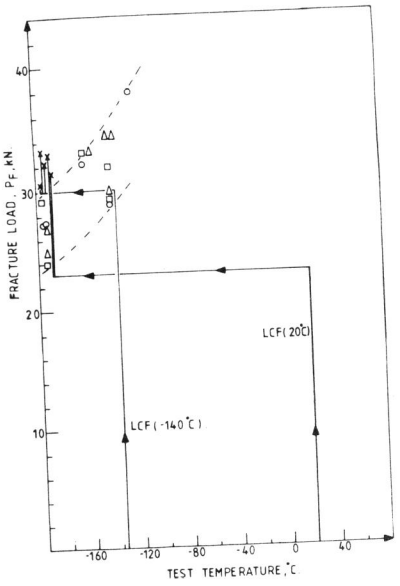

Fig. 10 WPS of blunt-notches - A508 (fully tempered condition).

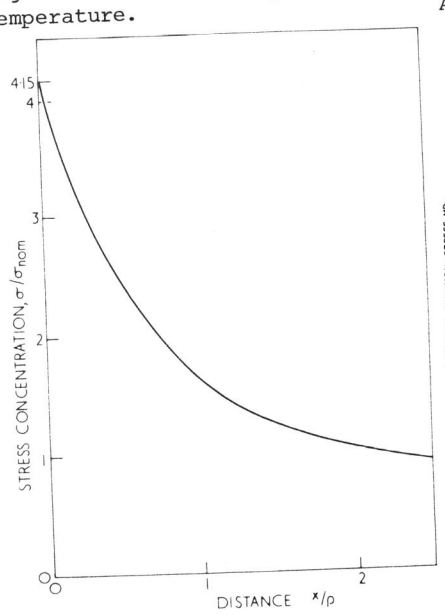

Fig. 11 Elastic stress concentration ahead of a blunt notch (after 10).

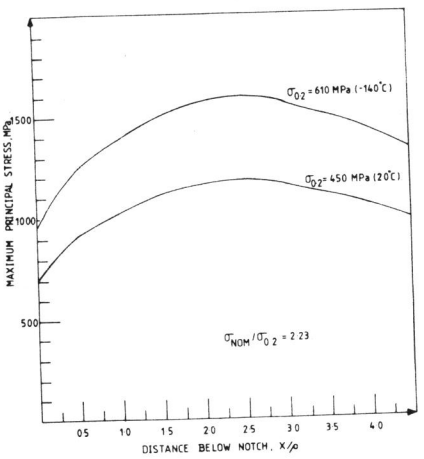

Fig. 12 Tensile stresses generated at -140 and 20°C for $\sigma_{nom}/\sigma_{0.2}$ = 2.23 (after 3).

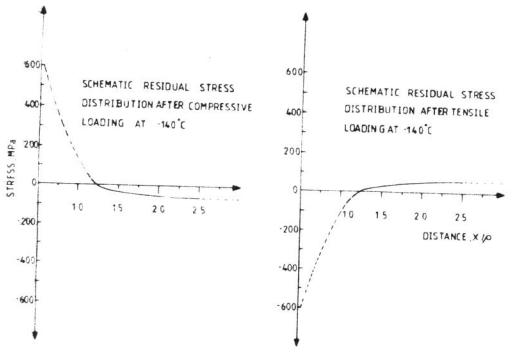

Fig. 13 Schematic residual stress distribution after prestressing at -140°C (A508, fully heat-treated condition).

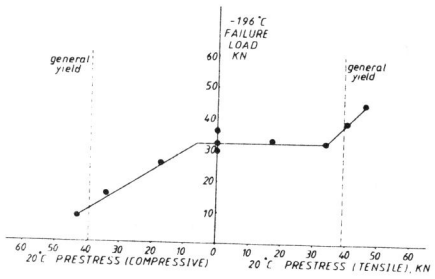

Fig. 14 LUCF results for A533B (non-fully tempered condition).

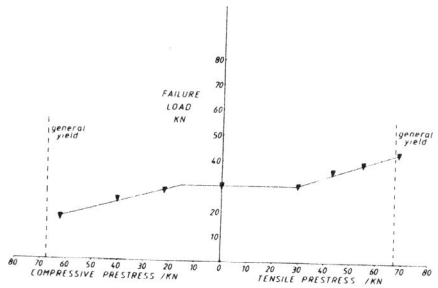

Fig. 15 LUCF results for high strength (martensitic) A533B.